Effect of Packing Density on the Surface Hydrophobicity of ω-Functionalized (–CF_3, –CH_3, –OCH_3, and –OH) Self-assembled Monolayers: A Molecular Dynamics Study

Hari O. S. Yadav,[1] *An-Tsung Kuo,*[2] *Shingo Urata,*[2] *and Wataru Shinoda*[1,*]

[1] Department of Materials Chemistry, Nagoya University, Furo-cho, Chikusa-ku, Nagoya 464-8603, Japan

[2] Innovative Technology Laboratories, AGC Inc., Yokohama, Kanagawa, 230-0045, Japan

* Email: w.shinoda@chembio.nagoya-u.ac.jp

Phone: +81-52-789-5288

ABSTRACT

The surface properties of self-assembled monolayers (SAMs) are generally determined by the terminal functional groups. However, variations in the chain flexibility or packing density of SAMs significantly affect the surface properties as well. In this study, we investigated the effect of the packing density on the surface hydrophobicity/hydrophilicity of ω-functionalized (–CF_3, –CH_3, –OCH_3, and –OH) SAMs using molecular dynamics simulations. The surface roughness and chain flexibility of these SAMs commonly increase with a decreasing packing density. The increase in the chain flexibility caused an enhancement in the surface hydrophobicity, regardless of the terminal groups. For SAMs with the CF_3 terminal, only the fluorocarbon segments were exposed to the surface at any packing density; thus, the surface roughness and chain flexibility were the only parameters that affected the surface hydrophobicity. Conversely, the surface (exposed) segments of the other SAMs were alternating depending on the packing density, altering the surface-water interfacial energies, which also contributed to a variation in the surface hydrophobicities. Therefore, the variation in the surface hydrophobicity of the SAMs due to the packing density was well characterized by considering the chain flexibility and exposed surface segments.

1. INTRODUCTION

Understanding the mechanism of protein adsorption on solid surfaces is important for the advancement of biotechnical and biomedical fields.[1] For example, biononfouling properties are desired for the design of a medical device, while certain interactions between the surface and specific biomolecules are required for bio-assay chips.[2-5] Techniques that involve self-assembled monolayers (SAMs) are employed to modify the functional groups at the surface and alter the surface properties; thus, they have been widely used to investigate the mechanistic aspects of the protein adsorption.[6-9] Through the SAM techniques, the adsorption behavior has been known to fundamentally related to the hydrophobic/hydrophilic characteristics of the surface. For instance, albumin has a stronger affinity to be adsorbed on the hydrophobic alkyl-terminated surface than on the hydrophilic hydroxyl- or carboxylate-terminated surfaces.[6, 8, 10-13] The antifouling and nonthrombogenic surfaces formed by zwitterionic, polyethylene glycol, and poly(2-methoxyethyl acrylate) based coatings are based on the low tendency of proteins to be adsorbed on hydrophilic surfaces.[5, 14-16]

The hydrophobic/hydrophilic characteristics of the surface originates from an interplay of the surface with water; thus, the composition of the SAM controls the hydrophobicity/hydrophilicity of the surface.[6] The surface roughness and lateral packing density also influence the hydrophobicity and protein adsorption. For example, a loosely packed alkyl-terminated SAM exhibited lower surface roughness and hydrophobicity, and greater adsorption of human serum albumin than a densely packed SAM.[17-18] Low-density carboxylate- and alcohol-terminated SAMs were more hydrophobic and adsorbed bovine serum albumin more easily than their analogous dense SAMs.[13]

Molecular dynamics simulations have been used to investigate the behavior of water at the interface with SAMs[19-25] and the adsorption behavior of proteins on the surface of SAMs.[26-29] The structure and dynamics of interfacial water molecules change depending on the

hydrophobic/hydrophilic characteristics of SAMs.[20-21,23] A hydrogen-bonding network between the hydrophilic SAM and water may be the main factor that prevents protein from adsorbing on the hydrophilic SAM.[19,26] In addition, the change in the packing density and chain flexibility can alter the strength of interfacial water-binding on the SAM and influence the protein adsorption.[28] Although most simulation studies aim to investigate the behavior of interfacial water and unravel the mechanism of protein adsorption on SAMs with highly smooth surfaces (densely packed SAMs),[26] several exceptions focus on the influence of the packing density and chain flexibility of SAMs.[25, 28, 30-31] Park *et al*. [30] simulated the behavior of water on a fluoroalkane SAM at various packing densities. Protein adsorption onto oligo(ethylene glycol) SAMs with different packing densities has also been reported by Beckner *et al*.[28] However, the mechanism by which the packing density and chain flexibility of SAMs with various terminal functional groups affect the behavior of the interfacial water has not yet been fully understood.

Poly(2-methoxyethyl acrylate) (PMEA) is an antifouling polymer used as a nonthrombogenic coating agent for artificial oxygenators. The water structure of hydrated PMEA has been suggested to play a critical role in its antifouling property.[5] Understanding the interplay between water and the surface of the PMEA analog will be useful for designing PMEA-based antifouling coatings. Recently, in-plane microphase separation to the polymer-rich and water-rich regions at the polymer/water interface has been found in PMEA-based coatings.[32-33] The polymer-rich domains (diameter of 50-100 nm) have demonstrated the higher tendency to adsorb the fibrinogen in comparison with the water-rich domains. The different capacities of adsorbing the fibrinogen were ascribed to the different polymer densities probably contributing to different hydrophobicities.[32-33] It is difficult not only to experimentally measure the difference in the hydrophobicity between polymer-rich and water-rich regions but also to directly simulate in-plane microphase separation at the polymer/water interface using molecular dynamics simulation. However, through the simulation of grafted side chain SAMs

with different packing densities, the difference in the physical properties between polymer-rich and water-rich regions can be qualitatively understood. Therefore, for understanding the interplay between water and the surface of the PMEA analog, we constructed SAMs formed of side chains of methacrylate-based polymers with four different terminal functional groups (as shown in Fig. 1) and investigated the interfacial properties between the SAMs and water. SAMs with these terminal groups present a wide variety of surface properties, ranging from hydrophobic to hydrophilic. We analyzed the interfacial properties, such as the surface hydrophobicity and hydrogen bonding between the water and SAM, as well as the structural properties of the surface. We considered a range of packing densities in the simulations and attempted to determine the effects of surface roughness and chain flexibility on the behavior of interfacial water for these chemically distinct surfaces.

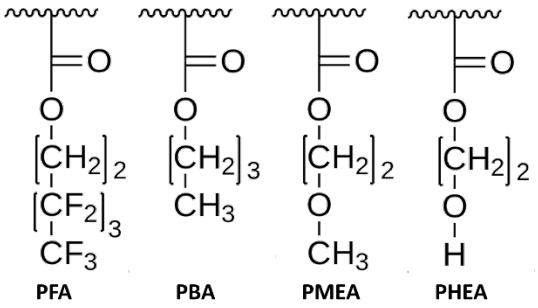

Figure 1. Side chains of poly(n-fluorobutyl acrylate) (PFA), poly(n-butyl acrylate) (PBA), poly(2-methoxyethyl acrylate) (PMEA), and poly(2-hydroxythyl acrylate) (PHEA).

2. METHODS

2.1. Computational details

To prepare the initial configurations of the SAMs, we first generated hexagonal close-packed two-dimensional (2D) lattices of fixed sites in the *xy* plane with different lattice parameters, a_0. The side chains of the polymers were then grafted to the fixed sites with an initial tilt angle

of 28° to form a grafted self-assembled monolayer surface. The arrangement of the chains with the initial tilt angle was based on alkanethiols adsorbed on the gold surface.[34] The chemical structures of the side chains are shown in Fig. 1. Three lattice parameters, 0.46, 0.50 and 0.59 nm, were chosen to control the packing densities of the SAMs. The choice of the lattice parameters is in consideration of the fact that the lattice spacings of hydrocarbon and fluorocarbon thiols chains on gold are 0.50 and 0.59 nm, respectively,[22] and molecular packing densities of oligoether-terminated SAMs on gold and silver are in the range from 2.7 to 5.0 molecule/nm^2.[35] Moreover, the spacings of 0.42 and 0.5 nm for the side chain crystalline of poly(n-alkylacrylate) and poly[(perfluoroalkyl)ethyl]acrylates, respectively, have been reported.[36-38] The lattice spacing of 0.46 nm is adopted to assume the formation of side chain crystalline on the surface. The lattice constants, a_0, and the corresponding packing densities, d_p, of the side chains are summarized in Table 1.

Table 1. Packing density, d_p, of surfaces corresponding to a given lattice parameter, a_0.

a_0 [nm]	d_p [chains/nm^2]
0.46	5.46
0.50	4.62
0.59	3.32

The packing density corresponds to the total number of chains in a monolayer divided by the surface area of the simulation box in *xy*-dimensions.

The side chains of the polymer were modeled using the all-atom OPLS force field.[39] The cross-dihedral interactions between hydrogenated and fluorinated segments of the PFA chain were based on Padua's research.[40] The SPC/E model was used for water molecules.[41] All simulations were performed in the canonical (NVT) ensemble at 300 K using the LAMMPS MD package.[42] The temperature was controlled using the Nosé-Hoover thermostat[43] with a time

constant of 1.0 ps, while the equations of atomic motion were integrated using the velocity Verlet algorithm with a time step of 1.0 fs. Water molecules were treated as rigid bodies using the SHAKE algorithm.[44-45] The short-range Lennard-Jones interaction was truncated at 1.0 nm, while the particle-particle particle mesh (PPPM) algorithm was used to calculate the electrostatic interactions.[46] The Visual Molecular Dynamics package was used to visualize the MD configurations.[47]

The initial structure of each SAM surface was first equilibrated under vacuum for 30 ns. During the calculation, an additional self-harmonic spring potential (4184 $kJ \cdot mol^{-1} \cdot nm^{-2}$) was applied for the root carbon of each chain in the SAMs to fix them at equally spaced positions on the same *xy* surface. To prevent the downward flipping of chains, which may happen especially at a low packing density, we placed a harmonic wall (with a spring constant of 4184 $kJ \cdot mol^{-1} \cdot nm^{-2}$) beneath the SAMs. The wall exerted a force when an atom tried to cross the position of the wall ($z = 0$); thus, it effectively worked as a repulsive solid substrate for the SAMs. For the SAM-water simulations, we took the final structure of the SAMs equilibrated under vacuum and placed a 3.5-nm thick water slab in the *z*-dimension of the SAM surfaces. The merged structures were equilibrated for 10 ns. Then, the simulation trajectories were stored at every picosecond over the next 20 ns and divided into 5 blocks to estimate statistical errors in the detailed analyses. The statistical errors for all quantities were less than 1.0% as shown in Fig. S3 of Supporting Information.

2.2. Simulation Analyses

A. Free Energy of Cavity Formation

The free energy of the cavity formation near the interface was calculated using the indirect umbrella sampling method proposed by Patel and Garde.[48-49] The cavity was created by

applying a harmonic biasing potential of a coarse-grained particle number, $\widetilde{N}_v$, of water molecules:

$$U(\widetilde{N}) = \frac{k}{2}\left(\widetilde{N}_v - N_v^*\right)^2, \quad (1)$$

where k is the spring constant and N_v^* defines the sampling window, i.e., the target number of coarse-grained water molecules in the probe volume, v. $\widetilde{N}_v$ is obtained using a truncated Gaussian function.[49] A series of simulations with different N_v^* were performed, and both the $\widetilde{N}_v$ and the actual number of water molecules, N, in the probe volume were monitored. Finally, an unbiased joint distribution function, $P_v(N)$, which was the probability of observing N water in the probe volume, was calculated using the unbinned weighted histogram analysis method[50] with samples from all simulations.

$$P_v(N) = \int P\left(N, \widetilde{N}_v\right) d\widetilde{N}_v. \quad (2)$$

The free energy of cavity formation, ΔA, is obtained as

$$\Delta A = -k_B T \ln P_v(0), \quad (3)$$

where k_B is the Boltzmann constant, and $P_v(0)$ is the probability of observing no water in the probe volume, v.

The simulation was performed using LAMMPS with the PLUMED package.[51] The spring force constant in biasing potential was 0.98 kJ/mol. The sampling window was determined using a similar method reported in the previous study.[49, 52-54] The detail was shown in Supporting Information. For each window, $\widetilde{N}_v^*$, the umbrella sampling was performed for 6 ns, in which we stored both $\widetilde{N}_v$, and the actual number of water molecules, N, in the probe volume at 1 ps increments. The unbiased joint distribution function, $P_v(N)$, was evaluated using the sampling of the last 5 ns, which was used to calculate ΔA (Eq. 3). ΔA is affected by the size and shape of the cavity together with the location from the surface. The cuboid cavity with 2.5 × 2.5 × 0.3 nm^3 was created at the half-density plane of water near the interface, as illustrated

in Fig. 2.[48-49, 55] The thickness of 0.3 nm is allowed to accommodate a water molecule of which diameter is around 0.28 nm, and large cross-sectional area is to obtain a large magnitude of the cavity formation free energy.[48] The cavity at the maximum density plane of water near the interface was also adopted to analyze the ΔA for comparison. The trends of ΔA are consistent with that analyzed by using cavity at the half-density plane of water near the interface as shown in Supporting Information.

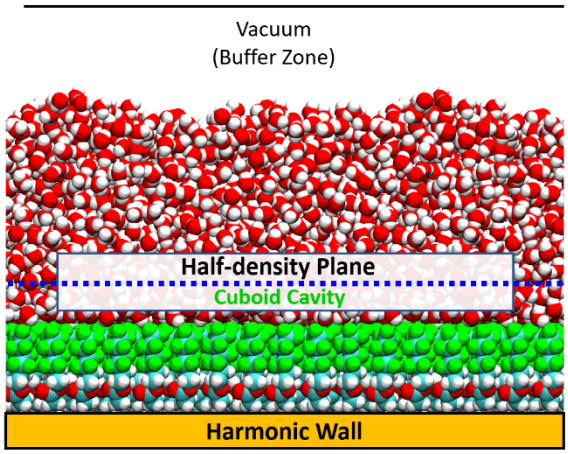

Figure 2. Cavity formation near the interface; the cavity of dimension, $v = 2.5 \times 2.5 \times 0.3$ nm^3 was created at the half-density plane, i.e., the center of the cavity where the water density along the surface normal was half of the bulk density, as shown by the blue dashed line.

B. Structure Properties

To obtain proper insight into the variation in the hydrophobicity of the surface, we investigated the structure of both water and SAMs using several metrics. The structural arrangement of water near the interface and its protrusion level in the SAM were examined by quantifying the mean density profile of atoms along the surface normal, z, as

$$\rho_w(z) = \frac{1}{A\Delta z}\langle\sum_{i=1}^{n}\delta(z_i)\rangle, \quad (4)$$

where A is the *x*-*y* surface area of the SAM, Δz is the bin width, $\delta(z_i)$ is the Kronecker delta function,[56] and n is the total number of water molecules.

We also calculated the number of hydrogen bonds between the surface and water molecules. A hydrogen bond is usually defined by the geometric criteria among all possible hydrogen acceptors (A), hydrogen donors (D), and hydrogen atoms (H). Here, we used the distance- and angle-based geometric criteria, i.e., the hydrogen bond was considered when the angle of the H, D, and A was less than 30°, and the distance between D and A was less than 0.35 nm simultaneously.[57]

The survival probability of water molecules near the surface was given by,[58]

$$P(\tau) = \frac{1}{t_{max}} \sum_{t=1}^{t_{max}} \frac{N(t,t+\tau)}{N(t)}, \quad (5)$$

where t_{max} is the maximum simulation time, τ is the time step, and $N(t, t+\tau)$ is the number of water molecules in the probe region during the time interval from t to $t+\tau$, and $N(t)$ is the number of water molecules at time t. We computed $P(\tau)$ in a 0.4 nm-thick water slab centered at the half-density plane placed parallel to the interface. The 0.4 nm-thick water slab was chosen following the previous works.[31, 59] This quantity revealed how long water molecules stayed near the interface; a slow decay of $P(\tau)$ meant a long residence time, and a fast decay suggested a short residence time of water molecules in the vicinity of a surface.

Furthermore, we computed the root mean square fluctuation (RMSF) of tail functional groups and the standard deviation in the distribution of tail functional groups along the surface normal. The former represented the chain flexibility, and the latter represented the root mean square roughness.[60]

3. RESULTS AND DISCUSSION

3.1. Free Energy of Cavity Formation

We evaluated the free energy of cavity formation, ΔA, to measure the hydrophobicity of the SAM surface constructed by grafted polymer side chains with different chemical functional groups and with different packing densities, d_p. The calculated ΔA values are plotted in Fig. 3. The order of ΔA for these SAMs was PFA and PBA < PMEA < PHEA at all packing densities. The ΔA near the SAM surface provides a measure of the hydrophobicity of the surface; namely, lower ΔA is expected for more hydrophobic surfaces. Thus, the results corroborated the higher hydrophobicity of the $–CF_3$ and $–CH_3$ surfaces, and the hydrophilicity of the –OH surface. The hydrophobicity of the surface with the $–OCH_3$ group was between those of the $–CH_3$ and –OH surfaces. The hydrophobicity trend is consistent with experimental observation.[6] The ΔA of the PFA and PHEA SAM surfaces decreased with a decreasing packing density, while those of the PBA and PMEA SAM surfaces increased (Fig. 3). This behavior indicated that the surface hydrophobicity of the PFA and PHEA SAM surfaces increased, and that of the PBA and PMEA surfaces decreased as the packing density decreased. The hydrophobicity trend of the $–CF_3$ and –OH SAM surfaces with the packing density are in agreement with the previous studies.[13, 30-31] The results demonstrated that the packing density had different effects on the hydrophobicity of SAM surfaces, depending on the functional groups. We further analyzed the surface-water interaction and surface structure of the SAMs to understand how the packing density affects the hydrophobicity of the SAM surface with various functional groups. The details are discussed in the following section.

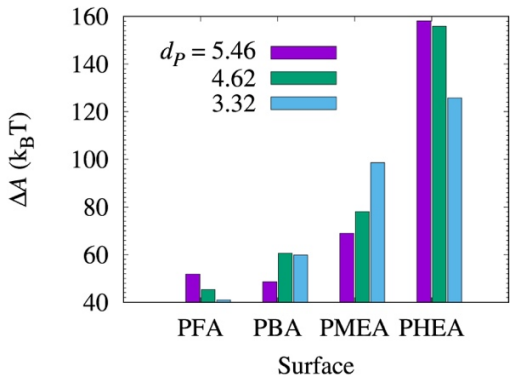

Figure 3. Free energy of cavity formation, ΔA, of SAM surfaces constructed by grafted polymer side chains with different functional groups and packing densities, d_p.

3.2. Surface Interaction and Morphology

Figure 4 plots the surface-water interaction energy, U_{tot}^{sw}, at different packing densities. U_{tot}^{sw} is simply calculated by the sum of the total van der Waals and electrostatic interaction between the grafted chains on the SAM and "all" water molecules.[57] U_{tot}^{sw} decreased for the PFA and PHEA surfaces and increased for the PBA and PMEA surfaces with a decreasing packing density. The variations in U_{tot}^{sw} for these SAMs as a function of the packing density were consistent with those of the ΔA. This result implied that the surface hydrophobicity of these SAMs at different packing densities was directly related to the interaction of the surface with water.

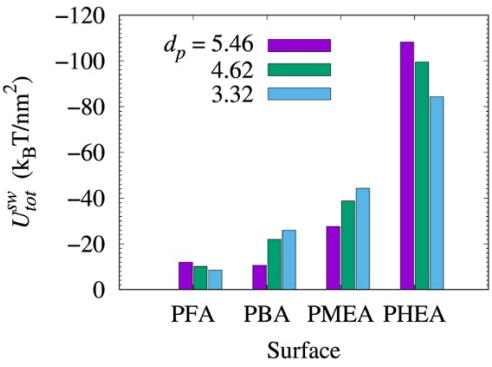

Figure 4. Surface-water interaction energy, U_{tot}^{sw}, of SAMs at different packing densities, d_p.

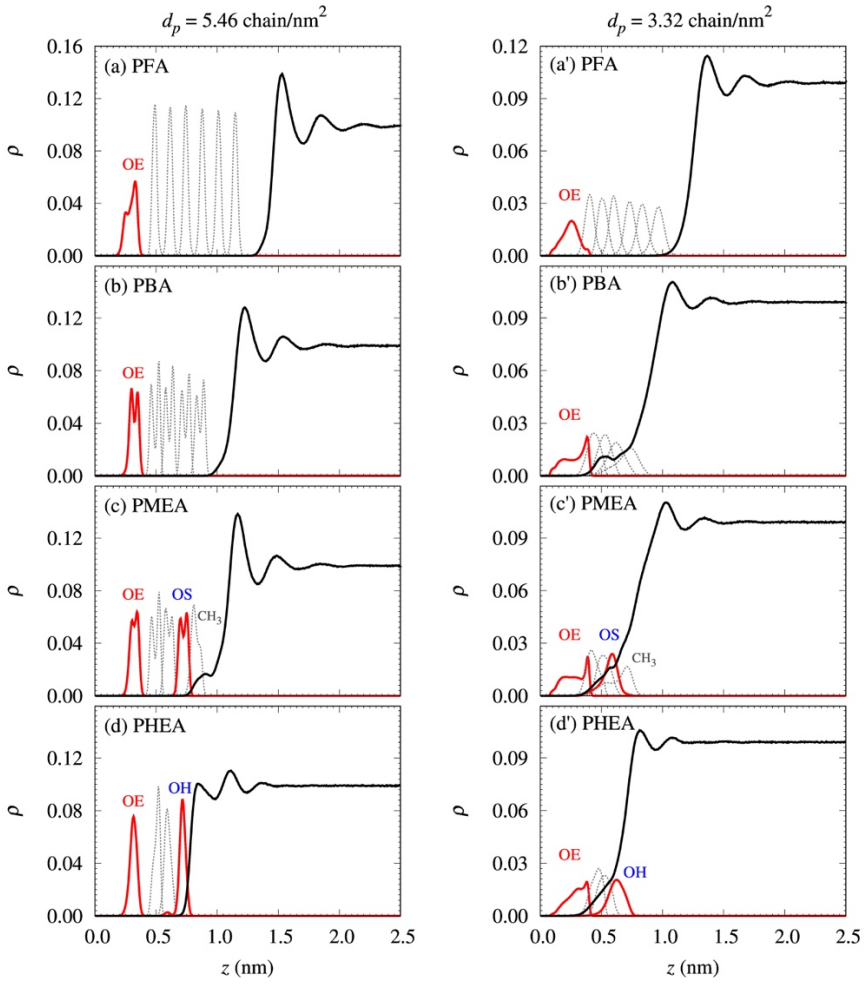

Figure 5. *Z*-density profiles of bulk water (black line), oxygen (red line), and carbon (black dashed line) atoms of side chains along the *z*-direction. (Left) d_p = 5.46 chains/nm^2, and (right) d_p = 3.32 chains/nm^2. OE: ester oxygen; OS: ether oxygen; OH: hydroxyl oxygen. The units of ρ is 10^3nm^{-3}.

The variation in the surface-water interaction energy may be ascribed to the fact that the interfacial composition could be effectively changed by changing the packing density. Therefore, we calculated the density profiles of bulk water $\rho(z)$ and heavy atoms of the side chains, and analyzed the hydrogen bonds between the surface oxygen and water molecules, as shown in Fig. 5 and 6, respectively. A slight overlap between the density profiles of water and ester oxygen was found for the PBA, PMEA and PHEA SAMs at d_p = 3.32 chains/nm^2 (Fig. 5). An increase in the hydrogen bonds between the ester oxygen and water molecules was also observed with a decrease in the packing density (Fig. 6a). This behavior indicated that a decrease in the packing density caused the water molecules to gradually penetrate the SAMs and directly associate with the ester groups. No hydrogen bonds were formed between the surface ester oxygen and water molecules when using the PFA SAMs. This behavior might appear because the fluorine atom possessed lower water affinity and more steric obstruction than the hydrogen atom. Thus, water molecules penetrated PFA SAMs with less ease than they do other SAMs.

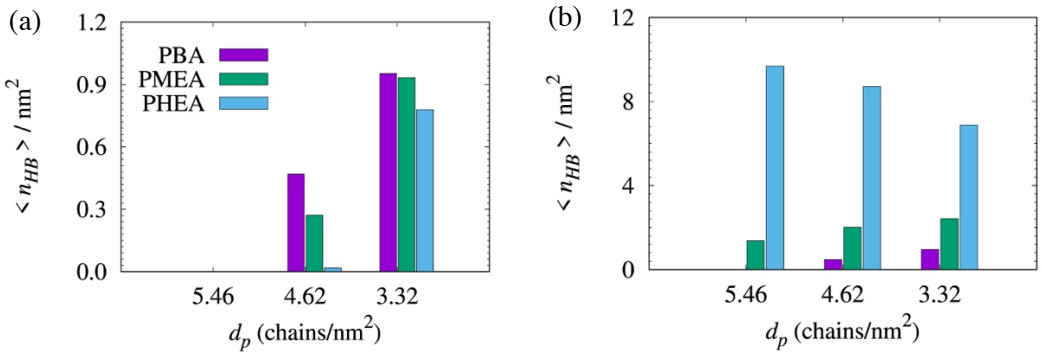

Figure 6. Average number of hydrogen bonds (a) between the ester oxygen and water molecules and (b) between the surface oxygen and water molecules. No hydrogen bonds were detected between the surface oxygen and water molecules on the PFA SAMs.

For the PFA SAMs, only fluorocarbon segments were exposed to the surface to interact with water at any packing density (Fig. 5). The interfacial component does not change with a change in the packing density. Thus, the variation in the surface-water interaction energy is not pronounced (less than $3k_BT$/nm^2, Fig. 4) even if the packing density is decreased from 5.46 chains/nm^2 to 3.32 chains/nm^2. However, the free energy of the cavity formation significantly decreased (Fig. 3), indicating an increase in surface hydrophobicity. This result implied that the other properties dominated the variation in surface hydrophobicity with the packing density for the PFA SAMs. In our previous study,[31] we performed a series of MD simulations to examine the surface hydrophobicity of PFA SAMs with different side-chain lengths; the results demonstrated that the surface roughness and chain flexibility affected the surface hydrophobicity of PFA SAM.[31] Specifically, the surface hydrophobicity increased with increasing surface roughness, while the increase in chain flexibility further enhanced the surface hydrophobicity by preventing water from staying near the interface.

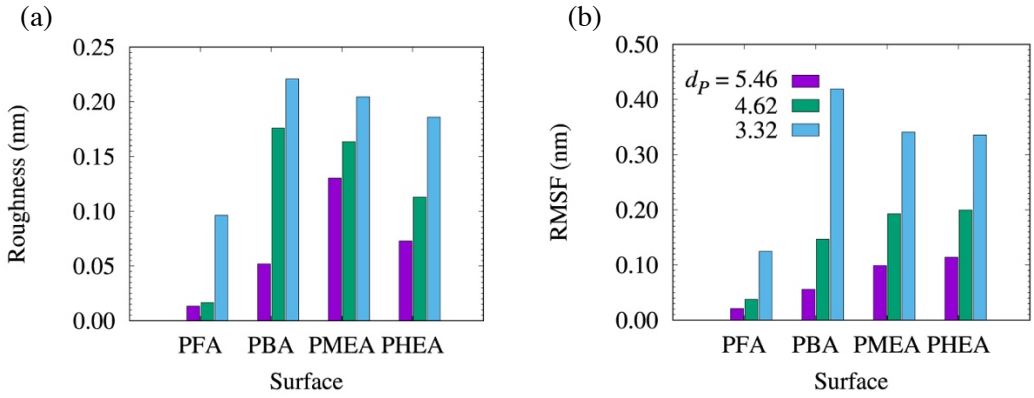

Figure 7. (a) Surface roughness and (b) root mean square fluctuation (RMSF) of tail atoms for SAMS at different d_p.

In the case of the PBA SAM, only hydrocarbon segments were exposed to the interface to contact water at d_p = 5.46 chains/nm^2. With a decreasing packing density, the bulk water could

gradually penetrate to z = 0.4 nm and form hydrogen bonds with the ester oxygen of the side chain. These hydrogen bonds contributed to the attractive interactions between the surface and water, reducing the surface hydrophobicity. We also calculated the surface roughness and RMSF of the tail atoms, which represent the chain flexibility, as shown in Fig. 7. When the packing density decreased, both the surface roughness and RMSF of the PBA SAM increased. This behavior should contribute to the enhancement of the surface hydrophobicity according to our previous study on the PFA SAMs.[31] However, the hydrophobicity of the PBA SAM decreased with a decreasing packing density (Fig. 3). These results demonstrated that the enhanced attractive interaction between the surface and water exceeded the effect of surface roughness and chain flexibility on the surface hydrophobicity of PBA SAMs.

The balance between surface-water interaction and surface structure is crucial for determining the overall hydrophobicity. Indeed, the difference in the surface-water interaction between the PBA and PFA SAM was minor (~1.5 k_BT) at d_p = 5.46 chains/nm^2, whereas the surface roughness and chain flexibility of the PBA SAM were significantly higher than those of the PFA SAM; this might cause the higher hydrophobicity on the PBA surface than on the PFA surface at d_p= 5.46 chains/nm^2.

For the PMEA SAM at d_p = 5.46 chain/nm^2, there is an overlap between the density profiles of bulk water and terminal –CH_3 groups but not between the density profiles of water and ether oxygen (Fig. 5(c)). Contrarily, a decreased packing density (3.32 chain/nm^2) (Fig. 5(c')) caused the distribution of ether oxygen to full overlap with that of water, illustrating that the ether oxygen was exposed to water. Although the methylene segments in between the ester oxygen and ether oxygen also gradually increased the amount exposed to the SAM surface, the interaction between hydrophobic methylene segment and water was expected to be similar to that between terminal methyl group and water. Thus, the ether oxygen exposed to water (Fig. 6) is the main source of the attractive interaction between the surface and water.

The z-density profile of the PHEA SAMs displayed that only the hydroxyl groups were exposed to the interface between the SAM surface and water at the highest packing density (5.46 chain/nm^2), while the other residue segments, such as the methylene segments, gradually increased the amount exposed to the interface between the SAM surface and water as the packing density decreased to 3.32 chain/nm^2 (Fig. 5 (d and d')). The increase in the content of the hydrophobic segments at the interface reduced the surface-water interaction energy.

The surface roughness of all SAMs increased with a decreasing packing density, as shown in Fig. 7. The increase in the surface roughness would increase the interfacial area and expose atoms from the middle of the side chains to the interface between the SAM surface and water. This behavior also reflected the variation in the interfacial composition, as discussed above.

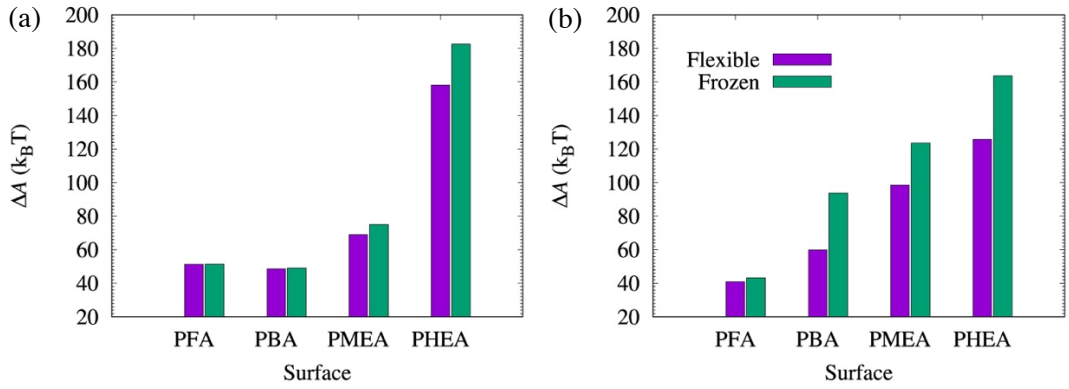

Figure 8. Cavity formation free energy of flexible and frozen surfaces: (a) d_p=5.46 and (b) d_p=3.32 chains/nm^2.

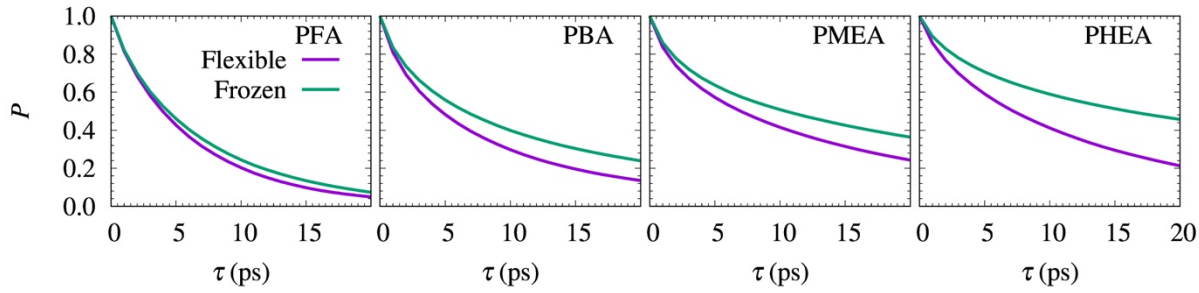

Figure 9. Analysis of the survival probability (or residence time) of water near the flexible and frozen surfaces at d_p=3.32 chains/nm^2.

To understand how chain flexibility affects the surface hydrophobicity of the PMEA and PHEA SAMs which possess hydrophilic groups, we restrained the positional fluctuations of chains on the surfaces (called frozen surfaces) by excluding the MD time integration of the SAM and estimated their hydrophobicity. Figure 8 shows ΔA of the SAMs with flexible (original) and frozen surfaces at d_p = 5.46 chains/nm^2 and 3.32 chains/nm^2. The ΔA of the flexible surfaces were lower than those of the frozen surfaces, indicating that flexible chains can enhance the hydrophobicity. To unravel the origin of the phenomenon, we analyzed the survival probability (or residence time) of water near the SAM surface (Fig. 9) and found that all flexible surfaces showed lower survival probability than the corresponding frozen surfaces. This behavior indicated that the mobile chains, regardless of the functional groups, enhanced water dynamics near the surface, and thus the flexible SAMs exhibited greater hydrophobicity.

The difference in ΔA between the frozen PMEA surfaces at d_p = 3.32 chains/nm^2 and 5.46 chains/nm^2 was approximately +48 k_BT, which was higher than the −25 k_BT and −6 k_BT values caused by the chain flexibility, which reduced water dynamics near the surface at d_p = 3.32 chains/nm^2 and 5.46 chains/nm^2, respectively. This behavior implied that the variation in the surface-water interaction due to the change in the packing density influenced the surface hydrophobicity more than the chain flexibility, reducing the surface hydrophobicity. The

differences in ΔA between the frozen PHEA SAM surfaces at d_p = 3.32 chains/nm^2 and 5.46 chains/nm^2 were approximately $-20\ k_BT$, which was smaller than $-38\ k_BT$ and $-24\ k_BT$ contributed by the chain flexibility at d_p = 3.32 chains/nm^2 and 5.46 chains/nm^2, respectively. This demonstrated that the influence of chain flexibility was more essential than that of the surface-water interaction energy. Figure 8 shows that the difference in ΔA between the frozen and flexible surfaces roughly increased with the decreasing hydrophobicity of the surfaces. This increase was ascribed to the fact that the energy variation for water leaving the hydrophilic surface was higher than that for water leaving the hydrophobic surface. Thus, the side chain with more hydrophilic properties contributed to the more pronounced chain flexibility effect; this may be the reason why the chain flexibility effect was more pronounced than that of the surface-water interaction energy on the PHEA SAM surface.

In summary, the packing density shows different effects on the surface hydrophobicity of SAMs with different functional groups. The surface roughness and chain flexibility increased with a decreasing packing density. The increase in the chain flexibility effectively enhanced the surface hydrophobicity regardless of the SAMs with hydrophobic or hydrophilic terminated groups. In addition, the increase in the surface roughness was expected to increase the probability of atoms in the middle of the side chains exposed to the interface between the SAM surface and water, possibly altering the interfacial composition depending on the functional groups on the SAM surfaces. Water could not penetrate the PFA SAMs to interact with ester oxygen and only interacted with the fluorocarbon segments at the interface; thus, the variation in the surface-water interaction with the change in the packing density was limited. Consequently, the surface roughness and chain flexibility are key factors that alter the surface hydrophobicity by adjusting the packing density. Water could penetrate the other SAMs and associate with ester oxygen at a lower packing density, changing the interfacial composition. The variation in the interfacial composition with the packing density substantially changed the

surface-water interaction. In conclusion, contrary to the PFA SAMs, the balance of the contributions from interfacial composition and chain flexibility controlled the surface hydrophobicity of the SAMs.

4. CONCLUSIONS

In this study, we investigated the surface hydrophobicity of four different SAMs at three different packing densities to identify the origin of the hydrophobicity of the SAM surfaces with hydrophobic and hydrophilic functional groups. The SAMs were constructed by grafting polymer side chains of PFA, PBA, PMEA, and PHEA. The surface hydrophobicity was characterized by examining the free energy of cavity formation and surface structure of the SAMs. The surface roughness and chain flexibility of all SAMs increased with a decreasing packing density. The former may change the interfacial composition depending on the functional groups of the SAM surfaces, and the latter can effectively enhance the surface hydrophobicity regardless of the hydrophobic or hydrophilic chains. In addition, the chain flexibility effect is more pronounced on the SAM surface constructed with hydrophilic chains. For the PFA SAMs, only fluorocarbon segments were exposed to the surface to contact with bulk water; thus, only the surface roughness and chain flexibility influenced the surface hydrophobicity. The other SAMs allowed water to penetrate them and associate with ester oxygens at low packing densities, changing the interfacial interaction. With a decreasing packing density, the increase in the probability of exposed oxygen atoms on the PBA and PMEA SAM surfaces increased the surface-water interaction energy. The effect of the interfacial composition overwhelms the effect of chain flexibility on the increase in water dynamics, causing a reduction in the surface hydrophobicity. Conversely, the increase in the probability of exposed ethylene groups on the PHEA SAM surface lowered the surface-water interaction energy. Both the interfacial composition and chain flexibility effects enhanced the

surface hydrophobicity and reduced the surface hydrophilicity of the PHEA SAM. In summary, this study explored the effect of the packing density on the surface hydrophobicity of the SAMs. The contribution balance among the surface roughness, interfacial composition and chain flexibility is crucial for determining the overall variation in the surface hydrophobicity relative to the packing density.

ASSOCIATED CONTENT

Supporting Information:

The Supporting Information is available free of charge on the ACS Publications website at DOI:

Additional details of the cavity formation free energy method (Fig. S1 – S3) and surface-water interaction energy.

AUTHOR INFORMATION

Corresponding Author

*Email: w.shinoda@chembio.nagoya-u.ac.jp. Phone: +81-52-789-5288

ACKNOWLEDGEMENTS

This research used the computational facilities of the supercomputer center at Nagoya University; Research Center for Computational Science, Okazaki; and the Institute for Solid State Physics, the University of Tokyo.

REFERENCES

(1) Rabe, M.; Verdes, D.; Seeger, S., Understanding Protein Adsorption Phenomena at Solid Surfaces. *Adv. Colloid Interface Sci.* **2011**, *162*, 87-106.

(2) Wu, G.; Datar, R. H.; Hansen, K. M.; Thundat, T.; Cote, R. J.; Majumdar, A., Bioassay of Prostate-Specific Antigen (Psa) Using Microcantilevers. *Nat. Biotechnol.* **2001**, *19*, 856-860.

(3) Situma, C.; Hashimoto, M.; Soper, S. A., Merging Microfluidics with Microarray-Based Bioassays. *Biomol. Eng.* **2006**, *23*, 213-231.

(4) Joddar, B.; Ito, Y., Biological Modifications of Materials Surfaces with Proteins for Regenerative Medicine. *J. Mater. Chem.* **2011**, *21*, 13737-13755.

(5) Tanaka, M.; Hayashi, T.; Morita, S., The Roles of Water Molecules at the Biointerface of Medical Polymers. *Polym. J.* **2013**, *45*, 701-710.

(6) Sigal, G. B.; Mrksich, M.; Whitesides, G. M., Effect of Surface Wettability on the Adsorption of Proteins and Detergents. *J. Am. Chem. Soc.* **1998**, *120*, 3464-3473.

(7) Sethuraman, A.; Han, M.; Kane, R. S.; Belfort, G., Effect of Surface Wettability on the Adhesion of Proteins. *Langmuir* **2004**, *20*, 7779-7788.

(8) Roach, P.; Farrar, D.; Perry, C. C., Interpretation of Protein Adsorption: Surface-Induced Conformational Changes. *J. Am. Chem. Soc.* **2005**, *127*, 8168-8173.

(9) Arima, Y.; Iwata, H., Effect of Wettability and Surface Functional Groups on Protein Adsorption and Cell Adhesion Using Well-Defined Mixed Self-Assembled Monolayers. *Biomaterials* **2007**, *28*, 3074-3082.

(10) Prime, K. L.; Whitesides, G. M., Adsorption of Proteins onto Surfaces Containing End-Attached Oligo(Ethylene Oxide): A Model System Using Self-Assembled Monolayers. *J. Am. Chem. Soc.* **1993**, *115*, 10714-10721.

(11) M Mrksich, a.; Whitesides, G. M., Using Self-Assembled Monolayers to Understand the Interactions of Man-Made Surfaces with Proteins and Cells. *Annu. Rev. Biophys. Biomol. Struct.* **1996**, *25*, 55-78.

(12) Silin, V.; Weetall, H.; Vanderah, D. J., Spr Studies of the Nonspecific Adsorption Kinetics of Human Igg and Bsa on Gold Surfaces Modified by Self-Assembled Monolayers (Sams). *J. Colloid Interface Sci.* **1997**, *185*, 94-103.

(13) Safazadeh, L.; Zehuri, V. E. F.; Pautler, S. P.; Hastings, J. T.; Berron, B. J., Relative Contribution of Lateral Packing Density to Albumin Adsorption on Monolayers. *Langmuir* **2016**, *32*, 8034-8041.

(14) Hoffman, A. S., Non-Fouling Surface Technologies. *J. Biomater. Sci. Polym. Ed.* **1999**, *10*, 1011-1014.

(15) Gudipati, C. S.; Finlay, J. A.; Callow, J. A.; Callow, M. E.; Wooley, K. L., The Antifouling and Fouling-Release Perfomance of Hyperbranched Fluoropolymer (Hbfp)–Poly(Ethylene Glycol) (Peg) Composite Coatings Evaluated by Adsorption of Biomacromolecules and the Green Fouling Alga Ulva. *Langmuir* **2005**, *21*, 3044-3053.

(16) Gao, C.; Li, G.; Xue, H.; Yang, W.; Zhang, F.; Jiang, S., Functionalizable and Ultra-Low Fouling Zwitterionic Surfaces Via Adhesive Mussel Mimetic Linkages. *Biomaterials* **2010**, *31*, 1486-1492.

(17) Sheller, N. B.; Petrash, S.; Foster, M. D.; Tsukruk, V. V., Atomic Force Microscopy and X-Ray Reflectivity Studies of Albumin Adsorbed onto Self-Assembled Monolayers of Hexadecyltrichlorosilane. *Langmuir* **1998**, *14*, 4535-4544.

(18) Choi, E. J.; Foster, M. D., The Role of Specific Binding in Human Serum Albumin Adsorption to Self-Assembled Monolayers. *Langmuir* **2002**, *18*, 557-561.

(19) Ismail, A. E.; Grest, G. S.; Stevens, M. J., Structure and Dynamics of Water near the Interface with Oligo(Ethylene Oxide) Self-Assembled Monolayers. *Langmuir* **2007**, *23*, 8508-8514.

(20) Yang, A.-C.; Weng, C.-I., Influence of Alkanethiol Self-Assembled Monolayers with Various Tail Groups on Structural and Dynamic Properties of Water Films. *J. Chem. Phys.* **2008**, *129*, 154710.

(21) Shenogina, N.; Godawat, R.; Keblinski, P.; Garde, S., How Wetting and Adhesion Affect Thermal Conductance of a Range of Hydrophobic to Hydrophilic Aqueous Interfaces. *Phys. Rev. Lett.* **2009**, *102*, 156101.

(22) Dalvi, V. H.; Rossky, P. J., Molecular Origins of Fluorocarbon Hydrophobicity. *Proc. Natl. Acad. Sci. U.S.A.* **2010**, *107*, 13603-13607.

(23) Xu, Z.; Song, K.; Yuan, S.-L.; Liu, C.-B., Microscopic Wetting of Self-Assembled Monolayers with Different Surfaces: A Combined Molecular Dynamics and Quantum Mechanics Study. *Langmuir* **2011**, *27*, 8611-8620.

(24) Guo, P.; Tu, Y.; Yang, J.; Wang, C.; Sheng, N.; Fang, H., Water-Cooh Composite Structure with Enhanced Hydrophobicity Formed by Water Molecules Embedded into Carboxyl-Terminated Self-Assembled Monolayers. *Phys. Rev. Lett.* **2015**, *115*, 186101.

(25) Dallin, B. C.; Van Lehn, R. C., Spatially Heterogeneous Water Properties at Disordered Surfaces Decrease the Hydrophobicity of Nonpolar Self-Assembled Monolayers. *J. Phys. Chem. Lett.* **2019**, *10*, 3991-3997.

(26) Stevens, M. J.; Grest, G. S., Simulations of Water at the Interface with Hydrophilic Self-Assembled Monolayers (Review). *Biointerphases* **2008**, *3*, FC13-FC22.

(27) Xie, Y.; Liu, M.; Zhou, J., Molecular Dynamics Simulations of Peptide Adsorption on Self-Assembled Monolayers. *Appl. Surf. Sci.* **2012**, *258*, 8153-8159.

(28) Beckner, W.; He, Y.; Pfaendtner, J., Chain Flexibility in Self-Assembled Monolayers Affects Protein Adsorption and Surface Hydration: A Molecular Dynamics Study. *J. Phys. Chem. B* **2016**, *120*, 10423-10432.

(29) Quan, X.; Liu, J.; Zhou, J., Multiscale Modeling and Simulations of Protein Adsorption: Progresses and Perspectives. *Curr. Opin. Colloid Interface Sci.* **2019**, *41*, 74-85.

(30) Park, S. H.; Carignano, M. A.; Nap, R. J.; Szleifer, I., Hydrophobic-Induced Surface Reorganization: Molecular Dynamics Simulations of Water Nanodroplets on Perfluorocarbon Self-Assembled Monolayers. *Soft Matter* **2010**, *6*, 1644-1654.

(31) Yadav, H. O. S.; Kuo, A.-T.; Urata, S.; Shinoda, W., Effects of Packing Density and Chain Length on the Surface Hydrophobicity of Thin Films Composed of Perfluoroalkyl Acrylate Chains: A Molecular Dynamics Study. *Langmuir* **2019**, *35*, 14316-14323.

(32) Murakami, D.; Kobayashi, S.; Tanaka, M., Interfacial Structures and Fibrinogen Adsorption at Blood-Compatible Polymer/Water Interfaces. *ACS Biomater. Sci. Eng.* **2016**, *2*, 2122-2126.

(33) Ueda, T.; Murakami, D.; Tanaka, M., Analysis of Interaction between Interfacial Structure and Fibrinogen at Blood-Compatible Polymer/Water Interface. *Front. Chem.* **2018**, *6*. 542

(34) Love, J. C.; Estroff, L. A.; Kriebel, J. K.; Nuzzo, R. G.; Whitesides, G. M., Self-Assembled Monolayers of Thiolates on Metals as a Form of Nanotechnology. *Chem. Rev.* **2005**, *105*, 1103-1170.

(35) Herrwerth, S.; Eck, W.; Reinhardt, S.; Grunze, M., Factors That Determine the Protein Resistance of Oligoether Self-Assembled Monolayers – Internal Hydrophilicity, Terminal Hydrophilicity, and Lateral Packing Density. *J. Am. Chem. Soc.* **2003**, *125*, 9359-9366.

(36) Platé, N. A.; Shibaev, V. P.; Petrukhin, B. S.; Zubov, Y. A.; Kargin, V. A., Structure of Crystalline Polymers with Unbranched Long Side Chains. *J. Polym. Sci. A-1 Polym. Chem.* **1971**, *9*, 2291-2298.

(37) Platé, N. A.; Shibaev, V. P., Comb-Like Polymers. Structure and Properties. *J. Polym. Sci. Macromol. Rev.* **1974**, *8*, 117-253.

(38) Honda, K.; Morita, M.; Otsuka, H.; Takahara, A., Molecular Aggregation Structure and Surface Properties of Poly(Fluoroalkyl Acrylate) Thin Films. *Macromolecules* **2005**, *38*, 5699-5705.

(39) Jorgensen, W. L.; Maxwell, D. S.; Tirado-Rives, J., Development and Testing of the Opls All-Atom Force Field on Conformational Energetics and Properties of Organic Liquids. *J. Am. Chem. Soc.* **1996**, *118*, 11225-11236.

(40) Pádua, A. A. H., Torsion Energy Profiles and Force Fields Derived from Ab Initio Calculations for Simulations of Hydrocarbon–Fluorocarbon Diblocks and Perfluoroalkylbromides. *J. Phys. Chem. A* **2002**, *106*, 10116-10123.

(41) Berendsen, H. J. C.; Grigera, J. R.; Straatsma, T. P., The Missing Term in Effective Pair Potentials. *J. Phys. Chem.* **1987**, *91*, 6269-6271.

(42) Plimpton, S., Fast Parallel Algorithms for Short-Range Molecular Dynamics. *J. Comput. Phys.* **1995**, *117*, 1-19.

(43) Martyna, G. J.; Tobias, D. J.; Klein, M. L., Constant Pressure Molecular Dynamics Algorithms. *J. Chem. Phys.* **1994**, *101*, 4177-4189.

(44) Ryckaert, J.-P.; Ciccotti, G.; Berendsen, H. J. C., Numerical Integration of the Cartesian Equations of Motion of a System with Constraints: Molecular Dynamics of N-Alkanes. *J. Comput. Phys.* **1977**, *23*, 327-341.

(45) Andersen, H. C., Rattle: A "Velocity" Version of the Shake Algorithm for Molecular Dynamics Calculations. *J. Comput. Phys.* **1983**, *52*, 24-34.

(46) Hockney, R. W.; Eastwood, J. W., Computer Simulation Using Particles; Adam Hilger: New York, **1989**.

(47) Humphrey, W.; Dalke, A.; Schulten, K., Vmd: Visual Molecular Dynamics. *J. Mol. Graphics* **1996**, *14*, 33-38.

(48) Patel, A. J.; Varilly, P.; Chandler, D., Fluctuations of Water near Extended Hydrophobic and Hydrophilic Surfaces. *J. Phys. Chem. B* **2010**, *114*, 1632-1637.

(49) Patel, A. J.; Varilly, P.; Chandler, D.; Garde, S.; Quantifying Density Fluctuations in Volumes of All Shapes and Sizes Using Indirect Umbrella Sampling. *J. Stat. Phys.* **2011**, *145*, 265-275.

(50) Tribello, G. A.; Bonomi, M.; Branduardi, D.; Camilloni, C.; Bussi, G., Plumed 2: New Feathers for an Old Bird. *Comput. Phys. Commun.* **2014**, *185*, 604-613.

(51) Tan, Z.; Gallicchio, E.; Lapelosa, M.; Levy, R. M., Theory of Binless Multi-State Free Energy Estimation with Applications to Protein-Ligand Binding. *J. Chem. Phys.* **2012**, *136*, 144102.

(52) Patel, A. J.; Garde, S., Efficient Method to Characterize the Context-Dependent Hydrophobicity of Proteins. *J. Phys. Chem. B* **2014**, *118*, 1564-1573.

(53) Xi, E.; Remsing, R. C.; Patel, A. J., Sparse Sampling of Water Density Fluctuations in Interfacial Environments. *J. Chem. Theory Comput.* **2016**, *12*, 706-713.

(54) Xi, E.; Marks, S. M.; Fialoke, S.; Patel, A. J., Sparse Sampling of Water Density Fluctuations near Liquid-Vapor Coexistence. *Mol. Simulat.* **2018**, *44*, 1124-1135.

(55) Godawat, R.; Jamadagni, S. N.; Garde, S., Characterizing Hydrophobicity of Interfaces by Using Cavity Formation, Solute Binding, and Water Correlations. *Proc. Natl. Acad. Sci. U.S.A.* **2009**, *106*, 15119-15124.

(56) Allen, M. P.; Tildesley, D. J., *Computer Simulation of Liquids*; Oxford University Press: New York, 1987.

(57) Ferrario, M.; Haughney, M.; McDonald, I. R.; Klein, M. L., Molecular-Dynamics Simulation of Aqueous Mixtures: Methanol, Acetone, and Ammonia. *J. Chem. Phys.* **1990**, *93*, 5156-5166.

(58) Liu, P.; Harder, E.; Berne, B. J., On the Calculation of Diffusion Coefficients in Confined Fluids and Interfaces with an Application to the Liquid–Vapor Interface of Water. *J. Phys. Chem. B* **2004**, *108*, 6595-6602.

(59) Li, E.; Du, Z.; Yuan, S., Properties of a Water Layer on Hydrophilic and Hydrophobic Self-Assembled Monolayer Surfaces: A Molecular Dynamics Study. *Sci. China Chem.* **2013**, *56*, 773-781.

(60) Gadelmawla, E. S.; Koura, M. M.; Maksoud, T. M. A.; Elewa, I. M.; Soliman, H. H., Roughness Parameters. *J. Mater. Process. Tech.* **2002**, *123*, 133-145.

TOC Figure: